Preparation of Al-doped xonotlite and its adsorption properties for Pb(II) in wastewater

Wenqing Tang[a,b], Youzhi Dai[a,c,d], Rongying Zeng[b,*], Biao Gu[b], Zhengji Yi[b], Zhiwei Liao[b], Zhimin Zhang[b], Huiyan He[b]

aSchool of Chemical Engineering, Xiangtan University, Xiangtan, Hunan 411105, China
bKey Laboratory of Functional Organometallic Materials of College of Hunan Province, College of Chemistry and Material Science, Hengyang Normal University, Hengyang, Hunan 421008, China, email: zengry13@163.com (R. Zeng)
cCollege of Environmental and Resources, Xiangtan University, Xiangtan, Hunan 411105, China
dHunan 2011 Collaborative Innovation Center of Chemical Engineering & Technology with Environmental Benignity and Effective Resource Utilization, Xiangtan, Hunan 411105, China

ABSTRACT

Al-doped xonotlite (Al-CSH) was prepared from SiO_2, $Ca(OH)_2$, and $NaAlO_2$ via the ultrasonic chemical method and doping technique for the removal of lead-containing simulated wastewater. The Al-CSH was analyzed by Brunauer–Emmett–Teller, scanning electron microscopy, and X-ray diffraction. The influence of solution pH, adsorption amount, contact time, initial concentration, and temperature were studied. The results showed that optimum adsorption conditions were found to be initial pH of 5.5, Al-CSH dosage of 0.06 g, initial Pb(II) ion concentration of 200 mg/L and contact time of 60 min. The adsorption capacity and removal rate of Al-CSH for Pb(II) ions was found to be 318.48 mg/g and 95.55% at optimum conditions. The adsorption isotherms followed the Langmuir isotherm model well. The adsorption processes were well fitted by the pseudo-second-order kinetic model. Thermodynamic studies indicated that the adsorption of Pb(II) by Al-CSH is spontaneous and endothermic. Mechanism studies revealed that Al-CSH removes lead ions from aqueous solution by ion exchange, surface precipitation, dissolution-precipitation, and electrostatic interactions. The results suggest that Al-CSH has the potential for use as an effective and low-cost sorbent for removing lead ions.

Keywords: Al-doped xonotlite (Al-CSH); Adsorption; Pb(II); Isothermal adsorption; Kinetics; Thermodynamics

1. Introduction

The demand for non-ferrous metals has increased with the rapid development of the economy and the advancement of industrialization. The ecological pollution caused by nonferrous metal has become an important environmental issue, which affects the quality of human health and attracts great attention from all countries [1–3]. Lead can accumulate in the liver and kidneys to cause anemia in hemoglobin synthesis disorders, thus interfering with the biochemical and physiological activities of the body. In some regions of Hunan, China, substandard industrial lead-containing wastewater has been discharged into natural water bodies, which seriously endangers local human health and life with events of blood lead.

Currently, the treatment methods of lead-containing wastewater mainly include chemical precipitation, ion exchange, membrane separation, biological method, electrocoagulation method, an adsorption method, etc. [4–10]. The chemical precipitation method is low in cost but easy to cause

* Corresponding author.

secondary pollution to the environment. The ion exchange method has more selectivity, but with high operation cost. The membrane separation technology, the biological method, and the electrocoagulation method are insufficient in efficiency but complicated in operation and high in cost. The adsorption methods have attracted much attention due to easy availability, low price, good removal effect, strong regenerability, and green concept in wastewater treatment [11,12]. For example, Yang et al. [13,14] used imprinted amino-functionalized mesoporous silica and Pb^{2+}, Cu^{2+} imprinted mesoporous adsorbents (Pb-IMA-UM and Cu-IMA-UM) as an adsorbent to remove lead, copper ions with an adsorption capacity of 217, 65.2, 198, and 51.5 mg/g, respectively; Fu et al. [15] used two-dimensional porous Fe_3O_4/poly $(C_3N_3S_3)$ as an adsorbent to remove lead ions with a maximum adsorption capacity of 232.6 mg/g. Therefore, in order to achieve high efficient separation process, the exploration of new adsorption materials is becoming more and more important.

The xonotlite $[Ca_6Si_6O_{17}(OH)_2]$ belongs to calcium silicate hydrate (C-S-H). As a good thermal insulation material, the xonotlite has been widely used in mining, electric power and construction fields. So there has been a lot of work in this field aimed at understanding the structural relations, formation mechanisms of the C–S–H phases. Some researchers have found that aluminum ions can be incorporated in the structure of hydrated calcium silicates, both at silicon and calcium sites [16,17]. Gabrovsek et al. [18] studied the influence of aluminum on the formation of tobermorite under hydrothermal conditions. The crystallization rate was found to increase with increasing aluminum content and temperature. The xonotlite has a large pore-like structure and large specific surface area. Some Chinese scholars used the hydrothermal method to prepare xonotlite. The xonotlite was applied in the treatment of heavy metal-containing wastewater because of cation exchange capacity, with obvious effects [19–22] and high removal rate. Miyake et al. [23] have found that Al–substituted gyrolite may be potentially useful for separation and waste disposal. Tsuji et al. [24] have reports concerning the complex substitution Al+Na, showing that tobermorite substituted in such a way exhibits the properties of an ion exchanger. It appears that Na and Al doping the calcium silicate hydrates (CSH) in formation and properties have significantly affected. However, there has been no report on the use of Al co-doped xonotlite for the removal of lead ions.

The common preparation methods of hydrated calcium silicate (C-S-H) mainly include chemical co-precipitation, sol-gel method, and hydrothermal method. The chemical co-precipitation and sol-gel methods are accompanied by partial secondary pollution. Ultrasonic-assisted hydrothermal method was used to avoid secondary pollution and realize the green synthesis. Ultrasonic chemistry is an important method for synthesizing nanomaterials developed in recent years. This method can control the morphology and size of particles, with broad application prospects [25,26]. Based on the ultrasonic chemistry method, we incorporated Na^+ and AlO_2^- instead of Ca^{2+} and SiO_4^{2-} in xonotlite for the first time to prepare Al-doped xonotlite (Al-CSH). Under static adsorption experiments, we determined the adsorption performance and adsorption mechanism of Pb(II) onto the Al-CSH. It provides an important theoretical reference for the application of lead-containing wastewater.

2. Materials and methods

2.1. Reagents and instruments

Analytically-pure reagents were used in the experiment. The 1 g/L Pb(II) stock solution was prepared from analytically-pure $Pb(NO_3)_2$ and deionized water. The other Pb(II) concentrations were obtained by dilution of the stock solution.

Main experimental instruments include Autosorb iQ specific surface area and pore structure tester (Conta Instruments, USA), EVO10 scanning electron microscope with energy spectrum (Germany Zeiss), Rigaku MiniFlex 600 X diffractometer (Rigaku, Japan), PH330i precision Acidity meter (WTW, Germany), TAS-990AFG atomic absorption spectrophotometer (Beijing General Instrument Co., Ltd.), and AD-6 automatic electronic balance (PE company of the US), Optima 2100DV ICP-MS, (PE company of the US).

2.2. Preparation and characterization of Al-doped xonotlite

2.2.1. Preparation of Al-doped xonotlit

According to the stoichiometric ratio of $n_{(Ca)}/n_{(Si+Al)}$ = 1.0 and $n_{(Al)}/n_{(Si+Al)}$ = 2%, 5%, 10%, or 15% the high dispersion suspension B (a certain amount of SiO_2 powder, 1.0 g KOH and 100 ml of deionized water) was slowly added dropwise to the high dispersion suspension A [0.1 mol of $Ca(OH)_2$ with 100 ml of deionized water] under the continuous action of ultrasonic waves at 50°C–60°C. Then, a certain amount of $NaAlO_2$ solution was slowly added. Next, 8.0 g NH_4HCO_3 was added as a blowing agent, for 30 min of ultrasonicated reaction, followed by 24 h of aging. The obtained product was washed successively with dilute hydrochloric acid, deionized water, and absolute ethanol. After that, it was dried, ground, and sieved to obtain Al-CSH$_1$ ~ Al-CSH$_4$ powder. Under the same conditions, four Al-CSHs were used to adsorb the wastewater containing lead ion. Al-CSH with $n_{(Al)}/n_{(Si+Al)}$ of 5% had the highest removal rate, reaching above 96%. Therefore, Al-CSH with $n_{(Al)}/n_{(Si+Al)}$ of 5% were selected as the experimental materials for the following studies, denoted as Al-CSH.

2.2.2. Characterization of Al-doped xonotlite sample

The Brunauer−Emmet−Teller (BET) specific surface area and pore size distribution of the sample were determined by N_2 adsorption on the adsorbent. BET equation was used to calculate specific surface area by N_2 adsorption isotherm. The phase analysis of the sample was performed on the X-ray diffractometer under the following conditions: the radiation source of Ka radiation excited by Cu target, the scanning range of 10°–80° (2θ) and the scanning speed of 4°/min. The surface morphology of the sample was observed by scanning electron microscopy (SEM).

2.3. Experimental methods

Batch adsorption experiments were performed by adding 0.02–0.12g of Al-CSH to 100 mL of 60–300 mg/L Pb(II) simulated wastewater into a 250 mL conical flask. The acidity and alkalinity were adjusted with HCl and NaOH. The mixture was shock (5–300 min) on a shaker at a constant temperature (293°K–313°K) and a rate of 150 r/min. After the reaction, it

was performed with centrifugal separation. Then, the supernatant was taken to determine the residual Pb(II) content. The removal rate ϱ(%) and the adsorption capacity Q_e (mg/g) were calculated as follows:

$$\rho = \frac{(C_0 - C_e)}{C_0} \times 100\% \qquad (1)$$

$$Q_e = \frac{(C_0 - C_e)V}{m} \qquad (2)$$

where C_0 is the initial concentration of Pb(II) (mg/L); C_e the equilibrium concentration of Pb(II) after adsorption (mg/L); V the volume of solution (L); m the amount of Al-CSH (g).

3. Results and discussion

3.1. Material characterization

The work characterized the specific surface area and porosity of pure xonotlite (CSH) and Al-CSH. Table 1 shows the specific surface area, average pore diameter, and average pore volume. According to the classification of porous materials, the pore size is mesoporous at 2–20 nm. It indicates that the xonotlite belongs to mesoporous material with large specific surface area, pore size, and pore volume, which is a good adsorption material. Table 1 shows that the specific surface area, pore-volume, and pore diameter of the modified Al-CSH are slightly larger than those of the unmodified CSH. This further demonstrates that the xonotlite can create a better adsorption environment through modification, with advantages in the adsorption of heavy metals. Therefore, the modified Al-CSH was selected for experiments on the adsorption of lead ions.

Fig. 1 shows the infrared spectroscopy results of xonotlite (CSH) and Al-CSH. The infrared spectrum shows that the structure of the modified material has not been destroyed, with the similar basic framework. The 3,300–3,700 cm^{-1} band is the stretching vibration absorption peak of –OH. Symmetric and asymmetric stretching vibration absorption peaks of Si–O–Si bond occur on 714.4 and 1,081.7 cm^{-1} bands, respectively. The two peaks of Si–O–Si bond are shifted to different extents, weakening the intensity of the two peaks to some extent. This may be due to the substitution of AlO_2^- for some SiO_3^{2-} in the xonotlite.

Fig. 2 shows the scanning electron micrograph of Al-CSH. The shape of the sample is similar to floc fiber. The needle-like surface is extremely rough, which is beneficial to the adsorption of the adsorbate in the solution due to fast contact with the active site of the Al-CSH surface. It indicates that this material is a good adsorbent material.

Table 1
BET data of CSH and Al-CSH

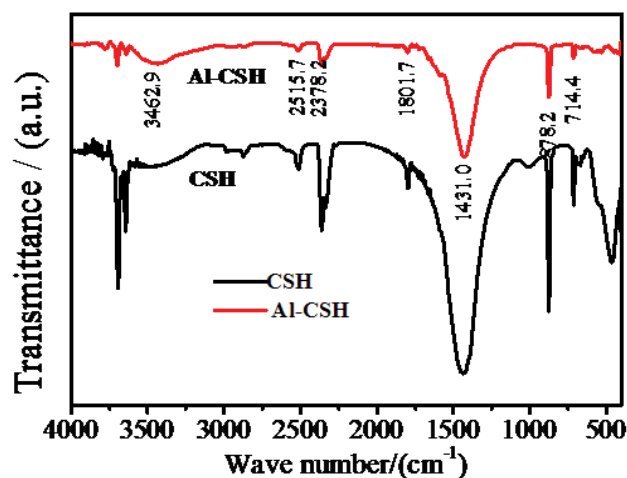| Sample	BET surface area (m²/g)	Average pore volume (cm³/g)	Average pore diameter (nm)
CSH	98.48	0.32	4.86
Al-CSH	136.72	0.48	5.76

Fig. 1. FTIR spectra of the CSH and Al-CSH samples.
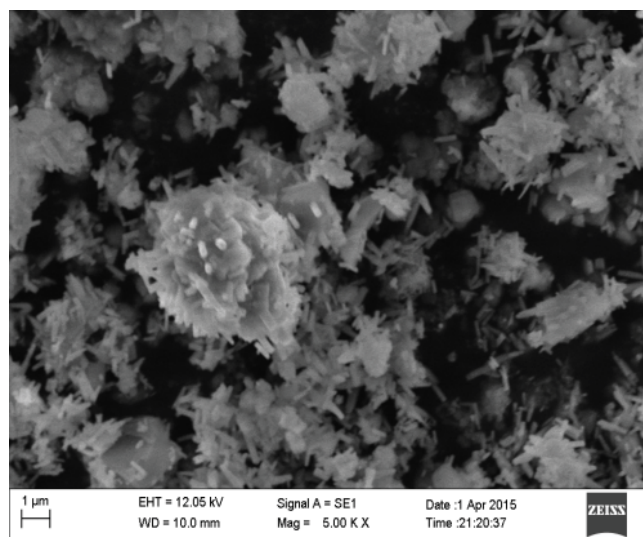

Fig. 2. SEM image of Al-CSH.

The energy spectrum (energy-dispersive x-ray spectroscopy, EDX) of Fig. 3 shows that the synthetic xonotlite sample material mainly composes of Ca, Si, and O. The peak of Al element significantly increases while that of Si element slightly decreases on the energy spectrum of the Al-CSH. This demonstrates that AlO_2^- is successfully doped in the CSH lattice, which replaces part of SiO_3^{2-} to form a new xonotlite derivative. In order to obtain the content of Al substitution, we have tested Al-CSH by ICP-MS to determine the exact percentage of Al and other elements in the formula. It was calculated that the contents of Al and Ca were 1.07 and 25.9%, respectively.

The crystal structure of Al-CSH was analyzed by X-ray diffraction (XRD; See Fig. 4). The XRD pattern of Al-CSH particles shows diffraction peaks around $2\theta = 20.8°$, 26.7°, and 29.4°, which is basically consistent with the standard diffraction pattern of xonotlite [27]. Meanwhile, the characteristic absorption peak of AlO_2^- appears at $2\theta = 23.0°$, 36.0°, and 36.5°, indicating that some AlO_2^- enter into the xonotlite
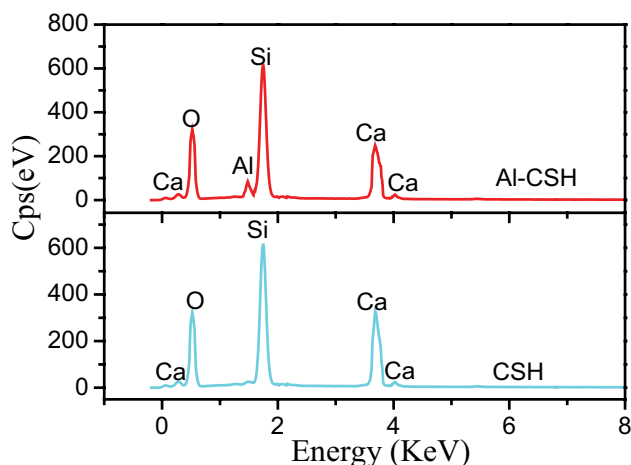
Fig. 3. EDX of CSH and Al-CSH.

Fig. 4. XRD of CSH and Al-CSH.

Fig. 5. Ratio of lead complex ions in different Ph.

Fig. 6. Adsorption of Pb(II) on Al-CSH as a function of pH in different NaNO$_3$ concentrations.
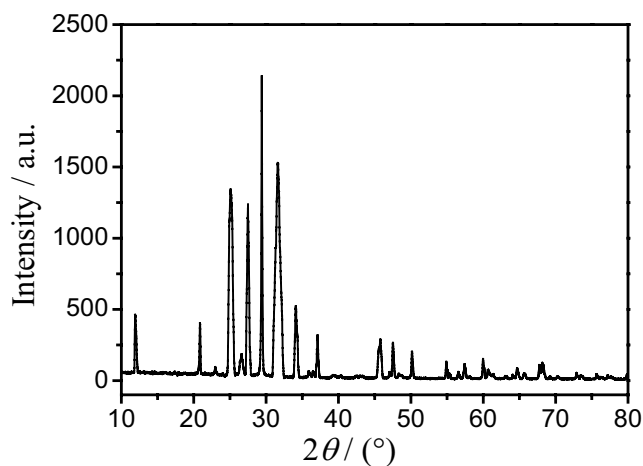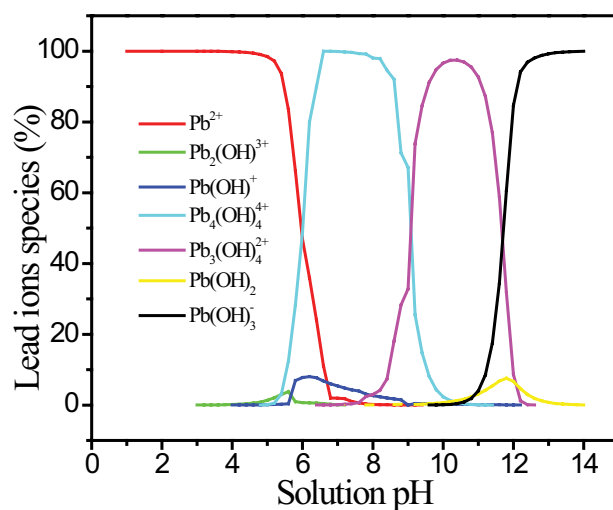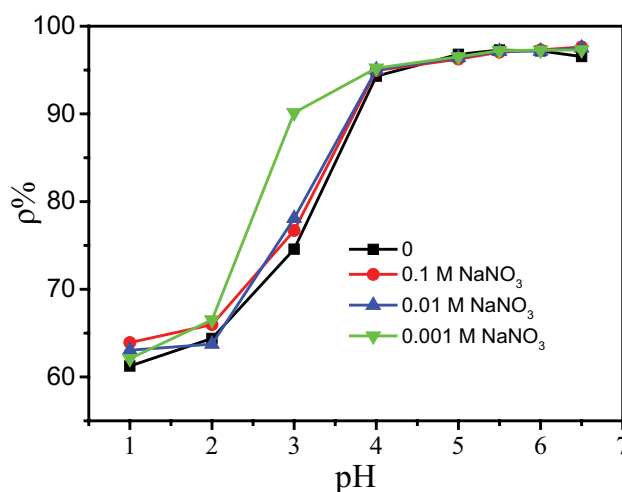
lattice to replace SiO_3^{2-}. Thus, the crystallinity of the particles is decreased to weaken the agglomeration.

3.2. Effect of pH on adsorption and ion strength

Figs. 5 and 6 show that the removal rate of Al-CSH for Pb increases continuously with the increase of pH in the range of 1.0–5.5, respectively. The main reason is that there is a large amount of H$^+$ and Pb^{2+} forming competitive adsorption in the acidic solution. H$^+$ is easily adsorbed to rapidly occupy the adsorption site on the surface of Al-CSH adsorbent, thus increasing the positive charge on the surface of the adsorbent. As a result, the positive charge generates repulsion with Pb^{2+} to inhibit the exchange and surface complexation of Pb^{2+}. The adsorption efficiency of Pb^{2+} onto Al-CSH is significantly decreased with the decline of pH value. At pH 5.5, the removal rate reached a maximum of 97.27%. The removal rate gradually decreases with a further increase in pH values of the solution. When pH > 5.5, the OH$^-$ in the solution increases to easily strengthen the hydrolysis of Pb(II)$^+$, resulting in the rapid transformation of Pb^{2+} to Pb(OH)$^{3+}$, Pb(OH)$^+$, and Pb$_4$(OH)$_4^{4+}$. The positively-charged ionic lead hydroxide

compounds repel Pb^{2+} due to the same charge. Then, Pb^{2+} is inhibited from reaching the Al-CSH surface for adsorption, reducing Al-CSH adsorption capacity for Pb(II). After the pH is further increased, sediments of Pb(OH)$_2$ occur in the solution, more against the adsorption of Pb(II). To investigate the effect of ionic strength on the adsorption of lead ions, the effect of different concentrations of NaNO$_3$ on the removal rate of lead ions was studied with Reference [28] (See Fig. 6). The result showed that the effect of ionic strength on the adsorption slightly declined, but without great impact on the whole. Therefore, the pH values were all set as 5.5 in other adsorption experiments of the work.

3.3. Effect of Al-CSH dosage on Pb(II) adsorption

According to the experiment method, the amount of adsorbent is adjusted for comparative experiments. Fig. 7 shows the change of removal efficiency for Pb(II) in solution
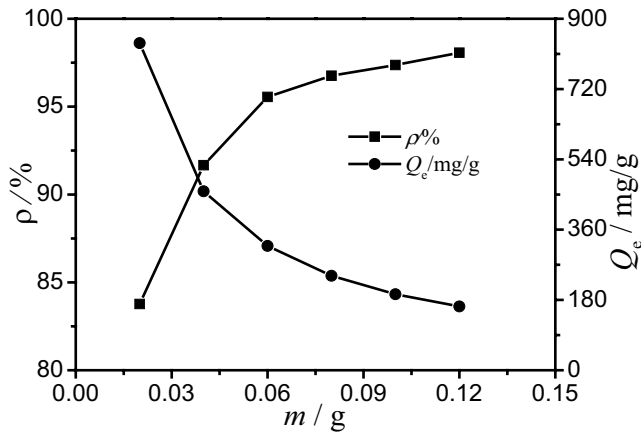
Fig. 7. Effect of Al-CSH dosage on the adsorption of Pb(II).

Fig. 8. Effect of initial Pb(II) concentration on adsorption at different temperatures.

with the dosage of adsorbent Al-CSH. The result indicates that the removal rate of Pb(II) firstly rapidly increases and then slowly increases with the rise of Al-CSH dosage; on the contrary, the trend of adsorption capacity changes from rapid decline to slow decrease. This is basically consistent with the adsorption law of similar adsorbents [29]. As the addition amount of Al-CSH increases from 0.02 to 0.06 g, the removal rate increases from 83.77% to 95.55%. Meanwhile, the adsorption capacity decreases from 837.7 to 318.4 8 mg/g. When the dosage of Al-CSH is further increased to 0.12 g, the removal rate and adsorption capacity become 98.07% and 163.44 mg/g, respectively. The removal rate of the adsorbent only increases by 2.52% compared with that of the dosage of 0.06 g, while the adsorption capacity has been decreased by 155.04 mg/g. After comprehensive comparison, the dosage of adsorbent used in the work was determined as 0.06 g to ensure higher removal rate and relatively large adsorption capacity.

3.4. Adsorption Models

3.4.1. Adsorption isotherms models

As an important method to reflect the adsorption characteristics of the adsorbate onto the adsorbent, the equilibrium adsorption isotherm is used to describe the adsorption capacity at different equilibrium concentrations. Meanwhile, the saturation adsorption capacity of the adsorbent can be obtained by fitting the adsorption process. Common isothermal equations include Langmuir isotherm (3), Freundlich isotherm (4), and Dubinin–Radushkevich (D–R) isotherm (5) [30,31].

$$Q_e = \frac{Q_m K_L C_e}{\left(1 + K_L C_e\right)} \tag{3}$$

$$Q_e = K_F C_e^{1/n} \tag{4}$$

where C_e is the concentration (mg/L) of Pb(II) in the solution when the adsorption reaches the equilibrium; Q_m the adsorption capacity (mg/g) when the adsorption reaches the equilibrium; Q_m the maximum adsorption amount (mg/g);
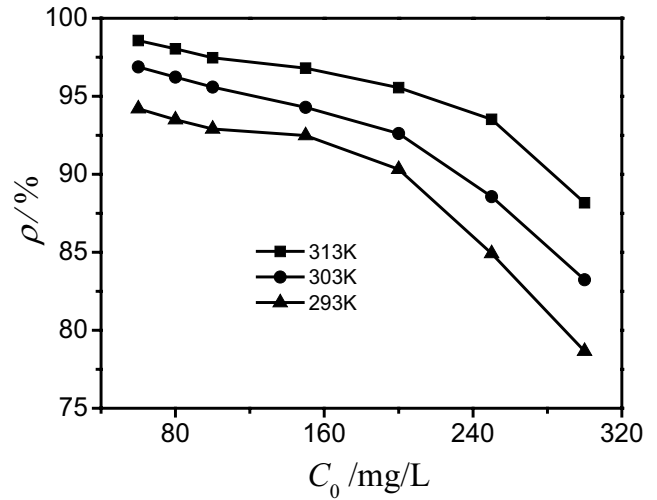
K_L the adsorption constant (L/mg) associated with adsorption energy; K_F and $1/n$ the Freundlich constants.

$$\ln Q_e = \ln X_m - k\varepsilon^2 \tag{5}$$

$$\varepsilon = RT \ln(1 + C_e^{-1}) \tag{6}$$

$$E = (2k)^{-1} \tag{7}$$

where C_e is the concentration of Pb(II) in the solution at absorption equilibrium (mol/L); k the model constant associated with free energy; X_m the monolayer adsorption capacity of the adsorbent (mol/g); ε the Polanyi potential energy (kJ/mol); R the universal gas constant kJ/(mol K); T the temperature (K); and E the change of average adsorption free energy (KJ/mol).

The adsorption experiment temperatures were controlled at 293, 303, and 313 K. The initial concentration of Pb(II) (60–300 mg/L) was changed for adsorption experiments. Fig. 8 shows the adsorption results of Pb(II) onto Al-CSH. It indicates that the removal rate of Pb(II) onto Al-CSH continually decreases at three temperatures with an increase of the initial concentration of Pb(II). The removal rate of high temperature is lower than that of low temperature, indicating that the rise of temperature is beneficial to the removal of Pb(II) onto Al-CSH within a certain temperature. In addition, it demonstrates that physical adsorption occurs in the adsorption mechanism besides chemical adsorption. The addition of energy promotes the combination of Al-CSH and Pb(II), thereby promoting the effective removal of Pb(II).

According to the experimental data of isothermal adsorption, the Langmuir, Freundlich, and D–R isothermal models were used to fit the adsorption process of Pb(II) onto Al-CSH. Fig. 9 show the fitting results, and Table 2 shows the fitting parameters. Comparing the results of three isothermal model fittings, the fitting coefficient of each isothermal model is higher than 0.9 within the experimental range, indicating that all the three isothermal models can reflect the adsorption behavior. Wherein, the
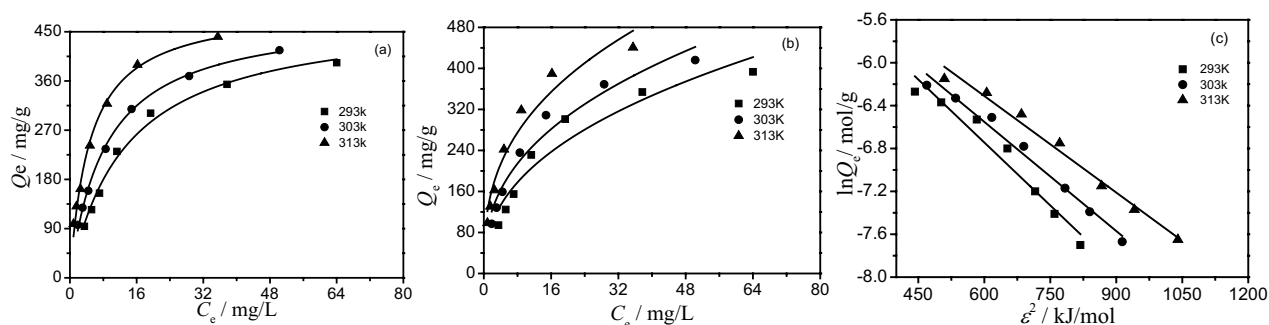
Fig. 9. Adsorption isotherm models (a) Langmuir isotherm, (b) Freundlich isotherm, and (c) Dubinin–Radushkevich model.

Table 2
Adsorption isotherm constants for Pb(II) onto adsorbents at various temperatures

Adsorbent Isotherm	Parameters	Temperatures (K)		
		293	303	313
Langmuir	Q_e (mg/g)	301.32	308.70	318.48
	Q_m (mg/g)	484.15	484.08	497.99
	K_L	0.0738	0.1162	0.2093
	R^2	0.9899	0.9974	0.9910
Freundlich	K_F	74.83	94.48	128.54
	$1/n$	0.4159	0.3938	0.3653
	R^2	0.9197	0.9555	0.9455
Dubinin–Radushkevich	X_m (mol/g)	0.0123	0.0109	0.011
	E (kJ/mol)	128.21	147.06	166.67
	R^2	0.9483	0.9807	0.9814

Langmuir isotherm model has the highest correlation coefficient (>0.98). It demonstrates that the Langmuir isotherm model is the most suitable model to describe the adsorption process, revealing that the adsorption is monolayer adsorption [30]. The larger Freundlich isotherm constant K_F value and the $1/n$ value of <1 indicate that the adsorption of Pb(II) onto Al-CSH belongs to preferential adsorption [32]. The E values of the mean adsorption free energy calculated by the D–R isothermal model are 128.21, 147.06, and 166.67 kJ/mol, respectively. This indicates that the adsorption of Pb(II) onto Al-CSH has the characteristics of ion exchange and surface complexation [31,33].

According to the saturated adsorption capacity Q_m of Pb(II) onto Al-CSH at different temperatures in Langmuir model, Q_m is larger at high temperature, indicating that temperature increase is beneficial to adsorption reaction. The saturated adsorption capacity of Pb(II) onto Al-CSH is up to 497.99 mg/g at 313°K. Table 3 shows the adsorption endothermic capacities of Pb(II) onto various adsorbents in recent literature. The adsorption capacity of CSH/chitosan is larger than that of the work, while the adsorption capacity of other materials is lower than of Al-CSH in adsorption of lead ions. It indicates that the Al-CSH adsorbent of the work has obvious advantages.

3.4.2. Adsorption kinetics

Equal kinetic models of Lagergren pseudo-first-order kinetics [See Eq. (8)], Lagergren pseudo-second-order kinetics [See Eq. (9)], Weber–Morris diffusion [See Eq. (10)], and Elovich [Eq. (11)] were used to further explore the adsorption mechanism of Pb(II) onto Al-CSH in solution [30].

$$Q_t = Q_e \left(1 - e^{-K_1 t}\right) \tag{8}$$

$$Q_t = \frac{Q_e^2 K_2 t}{(1 + Q_e K_2 t)} \tag{9}$$

$$Q_t = K_i t^{1/2} + C \tag{10}$$

$$Q_t = \frac{1}{\beta_e \ln(\alpha_e \beta_e)} + \frac{1}{\beta_e \ln t} \tag{11}$$

where Q_t is the adsorption amount (mg/g) at time t; K_1 the pseudo-first-order adsorption rate constant (min^{-1}); K_2 the pseudo-second-order adsorption rate constant [mg/(g min)]; K_i the internal diffusion adsorption rate constant (mg/g min$^{1/2}$); C the constant; α_e [mg/(g min)] the initial

Table 3
Comparison of adsorption capacity for Pb(II) by various adsorbents

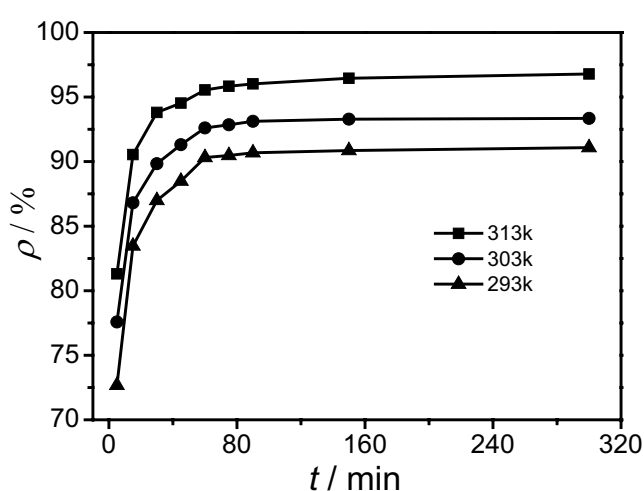| Adsorbent	pH	Initial Pb^{2+} concentration	Q_m (mg/g)	References
CSH/chitosan	8.0	100 mg/L	796.0	[34]
HAP/CSH	5.0	207.2 mg/L	462.0	[28]
Mild air oxidation of a biochar	5.0	100 g/m^3	7.9	[29]
CoFe$_2$O$_4$ nanoparticles	6.0	50–300	326.79	[35]
Plant biochar	5.0	30–500 mg/L	138.9	[36]
Cr-pillared clays	6.0	10–1300 mg/L	222.22	[37]
Mesoporous silica	5.5	200 ppm	48.3	[38]
Al-CSH	5.5	60~300	497.99	This work

Fig. 10. Effect of contact time on the adsorption of Pb(II) onto Al-CSH at different temperatures.

adsorption rate constant; β_e (g/mg) the desorption rate constant.

Comparative adsorption experiments of Pb(II) onto Al-CSH were implemented under 293, 303, and 313°K, respectively. Fig. 10 shows the changing trend of the removal rate with the contact time. It indicates that the removal rate of Pb(II) onto Al-CSH increases rapidly from 70% to over 90% in the early adsorption stage of 5–60 min, with a fast adsorption rate. In the late stage within 60–300 min, the removal rate and adsorption capacity of Pb(II) onto Al-CSH increased steadily, with the removal rates increased by only 1.5%, 1.67%, and 2.28% at three temperatures, respectively. The increase is not significant, which demonstrates that the adsorption of Pb(II) onto Al-CSH is close to equilibrium at 60 min. The increase of adsorption time has little effect on improving the adsorption. In the early stage of adsorption, most of Pb(II) is adsorbed on the surface of Al-CSH due to electrostatic action. Meanwhile, ion exchange and surface complexation occur between some lead ions and calcium ions. At the late stage of adsorption, most of the adsorption sites on the adsorbent surface were occupied by Pb. (II), leading to the weakening of adsorption force and reduction of adsorption rate. Therefore, the adsorption time in the work was controlled as 60 min.

The experimental data on adsorption of Pb(II) onto Al-CSH at 293, 303, and 313°K were fitted (See Fig. 11). Table 4 shows the fitting results.

The adsorption experiment data was fitted (See Table 4). Comparing the results of fitting parameters in four kinetic models, where the pseudo-second-order model has the best fitting effect, with the correlation coefficient R^2 of above 0.99. Meanwhile, the theoretical adsorption capacity $Q_{e,cal}$ calculated by the pseudo-second-order kinetic equation is consistent with that obtained from the experiment. The model can well describe the adsorption of Pb(II) onto Al-CSH, and it also proves that the adsorption has chemisorption behavior [39].

The parameter intercept is not equal to zero in the Weber–Morris diffusion (Internal divergence) fitting model. The straight-line does not pass through the origin, indicating that the internal diffusion process is not a single control step of the adsorption rate. It is inferred that the adsorption contains the integrated control process containing multiple effects such as external liquid film diffusion, surface adsorption, and internal diffusion of particles [40]. In addition, the K_i of the internal diffusion equation decreases with increasing temperature, while the equilibrium adsorption capacity of Pb(II) increases accordingly. It proves that the rise of temperatures in the adsorption process is conducive to the adsorption reaction and effective improvement of the removal of Pb(II). The larger slope and intercept of the model obtained by Elovich fitting demonstrates that Al-CSH has a fast adsorption rate and strong adsorption capacity for Pb(II).

3.4.3. Adsorption thermodynamics study

The adsorption thermodynamics reflects the thermal effect of the adsorption process under isothermal isostatic pressure. Endothermic or exothermic characteristics can be presented. Meanwhile, it indirectly judges whether the process is spontaneously performed. The main parameters of adsorption thermodynamics include Gibbs free energy (ΔG), enthalpy change (ΔH), and entropy change (ΔS). The positive or negative value of ΔG can determine whether the reaction is performed spontaneously; the positive or negative value of ΔH determines whether the reaction is an endothermic or exothermic process. The thermodynamic parameter values were calculated from Eqs. 12–15 [41,42]:

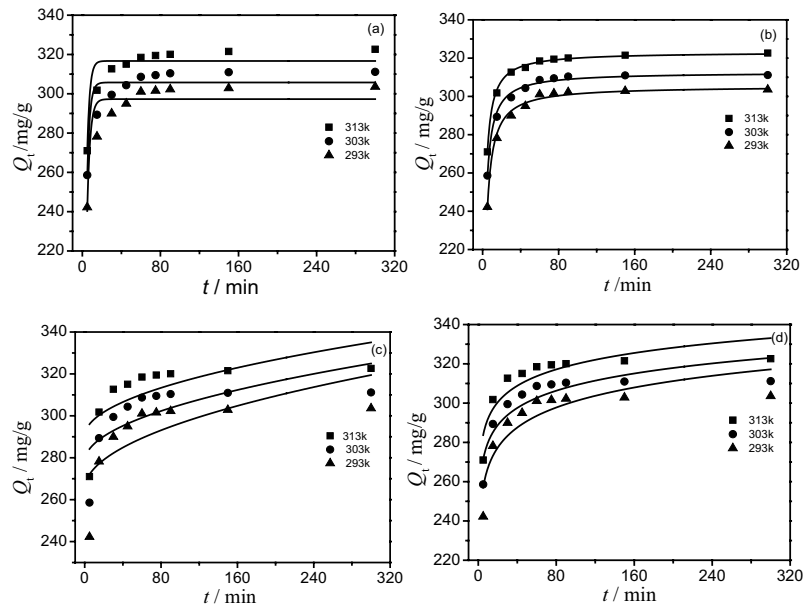$$\Delta G = \Delta H - T\Delta S \tag{12}$$

Fig. 11. Adsorption kinetics models (a) pseudo-first-order model, (b) pseudo-second-order model, (c) Weber–Morris diffusion model, and (d) Elovich model.

Table 4
Comparison of the different kinetic model parameters

Kinetics models	Parameters	Temperatures (K)		
		293	303	313
Pseudo-frist-order	$Q_{e,exp}$ (mg/g)	301.32	308.70	318.48
	$Q_{e,cal}$ (mg/g)	297.26	305.76	316.70
	K_1	0.3306	0.3691	0.3833
	R^2	0.8288	0.8191	0.8448
Pseudo-second-order	$Q_{e,cal}$ (mg/g)	305.40	312.64	323.17
	K_2	0.0024	0.0030	0.0032
	R^2	0.9912	0.9902	0.9970
Weber–Morris diffusion	K_i	3.1460	2.7053	2.5880
	C	264.97	278.11	290.21
	R^2	0.4427	0.4428	0.4427
	β_e	0.0677	0.0791	0.0830
Elovich	α_e	1.15×10^8	5.21×10^9	4.03×10^{10}
	R^2	0.7825	0.7836	0.7787

$$\Delta G = -RT \ln K_0 \tag{13}$$
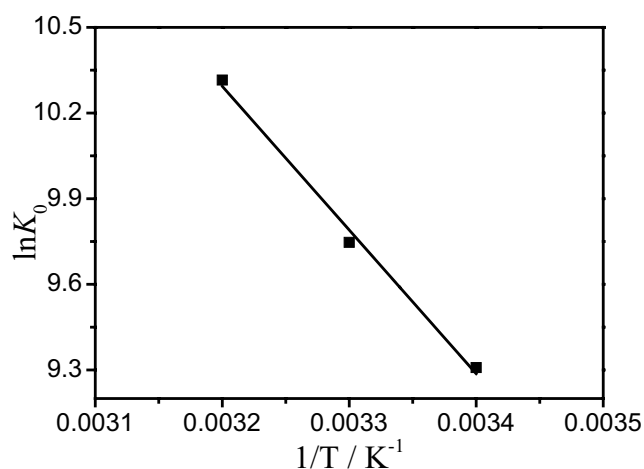
$$\ln K_0 = 1{,}000 \times C_0 \times \ln K_L \tag{14}$$

$$\ln K_0 = \frac{-\Delta H}{(RT)} + \frac{\Delta S}{R} \tag{15}$$

where R is the gas constant [J/(mol × K)]; T the absolute temperature (K); K_0 the equilibrium constant characterizing the distribution of Pb(II) between the solution phase and the adsorbent material; K_L the Langmuir constant.

Linear regression is performed for $\ln K_0$ and $1/T$. Fig. 12 shows the linear fitting equation is $Y = -5{,}212X + 27.33$, with the correlation coefficient of $R^2 = 0.9890$ Gibbs free energy (ΔG), enthalpy change (ΔH), and entropy change (ΔS) in the actual state were calculated according to Eqs. (16) and (17).

Table 5 shows that ΔG values in the thermodynamic parameters are all negative, indicating that the adsorption of Pb(II) onto Al-CSH in the solution is spontaneously performed. The enthalpy change value is used to judge the type of adsorption. The enthalpy change of chemical adsorption is usually >60 KJ/mol, while that of physical adsorption is generally <40 KJ/mol. The ΔH in adsorption of Pb(II) onto

Fig. 12. Relationship curve of $\ln K_0$ vs. T^{-1}.

Fig. 13. Effect of acid treatment on the lead extraction efficiency from the Al-CSH.

Table 5
Thermodynamic parameters at different temperatures

Adsorbent	T(K)	ΔG kJ/mol	ΔH kJ/mol	ΔS J/(mol K)
Al-CSH	293	−22.46		
	303	−24.66	41.87	219.55
	313	−26.85		

Al-CSH is >40 KJ/mol, demonstrating that the adsorption is an endothermic reaction process. Thus, we can conclude that the rise of temperature is conductive to the adsorption reaction. Meanwhile, the adsorption mechanism of Pb(II) onto Al-CSH is the comprehensive adsorption behavior of ion exchange, surface complexation and physical adsorption [41], which is basically consistent with the results of the previous isothermal adsorption model. A positive value of entropy indicates an increase in the irregularity of the adsorption process [33].

3.5. Regeneration

The Al-CSH sample after adsorption of Pb(II) was desorbed by 50 mL 0.1 mol/L hydrochloric acid. After desorption, the sample was washed and filtered four times with deionized water, dried at 70°C. Then, the Pb(II) adsorption experiment was repeated five times in sequence according to the experimental method. Fig. 13 shows the experimental results. From the cycling desorption-adsorption experiments, we find that the removal rate in adsorption of Pb(II) onto Al-CSH still maintains a high value of 88.67% after five times of regenerations, only decreasing by 6.88%. This demonstrates that the material has good adsorption performance, with high regenerative capacity and impact resistance.

3.6. Possible adsorption mechanisms studies

Guan et al. [43] found that calcium silicate hydrate near the surface had the concentration of Ca^{2+}, OH^-, and

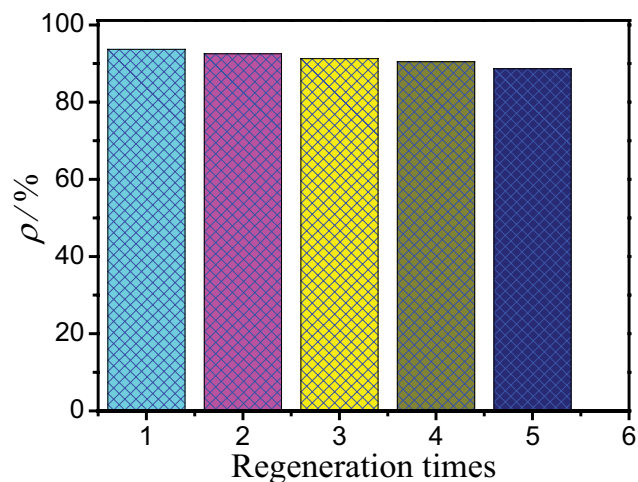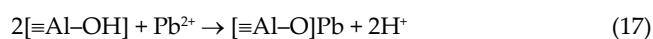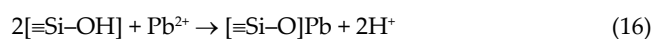$H_3SiO_4^-$ by the flow field distribution characteristics. Calcium silicate hydrate could the release of Ca^{2+} and OH^- via solubility experiments [43,44]. The study also found that calcium silicate hydrate contains Ca–OH bonds as well as Si–OH bonds [45]. Al-CSH is one of hydrous CSH, also contains Ca–OH, Si–OH, and Al–OH bonds. Al-CSH near the surface in solution also existed Ca^{2+} and OH^-, Pb(II) can exchange Ca^{2+}, similar to the result was reported elsewhere in the calcium silicate hydrate [46] and the hydroxyl groups on the surface can combine the heavy metal ions by chemical adsorption [28,47,48]. Through this result, we can speculate that there are surface complexation reaction between lead ions and Al-CSH.

$$2[\equiv Si–OH] + Pb^{2+} \rightarrow [\equiv Si–O]Pb + 2H^+ \qquad (16)$$

$$2[\equiv Al–OH] + Pb^{2+} \rightarrow [\equiv Al–O]Pb + 2H^+ \qquad (17)$$

At high pH values, only less H^+ (or H_3O^+) ions exited in solution, the existence of $\equiv Si–O^-$ and $\equiv Al–O^-$ groups on the A-CSH surface were speculated [28,47,48], form static adsorption with the positive charge taken by lead ions.

As seen from the SEM and EDX after adsorbing in Figs. 14a and b, the surface of Al-CSH are similar to the floc fiber and the needle-like surface, which suggests that Al-CSH has a large adsorption surface area. Compared with the SEM before and after adsorbing Pb^{2+} (Figs. 2 and 14), the results indicated that the adsorption of Pb^{2+} mainly occurred on the outer surface of Al-CSH and it was probable for the formation of Pb precipitates [47].

In summary, the possible mechanisms involved in Pb^{2+} sorption by Al-CSH may be divided into three parts (Fig. 15): ion exchange followed by surface complexation, dissolution-precipitation, and electrostatic interactions.

3.7. Cost estimation of Al-CSH production

A synthetic cost analysis was performed on Al-CSH to evaluate the economic feasibility. Without considering the electricity and labor costs, the main raw materials collected
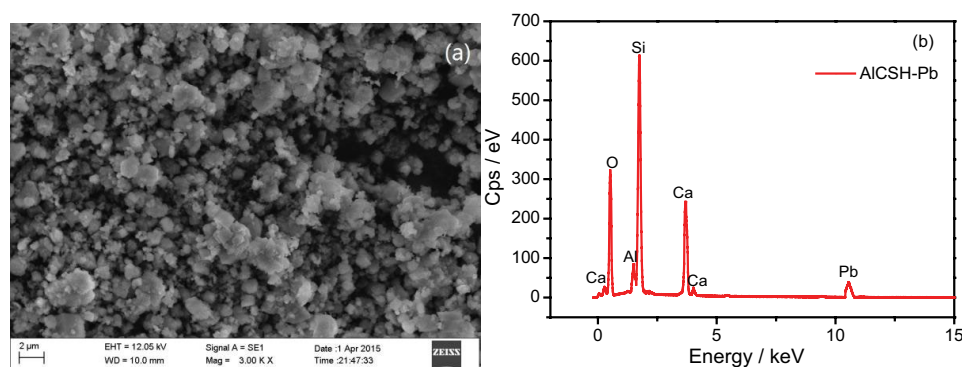
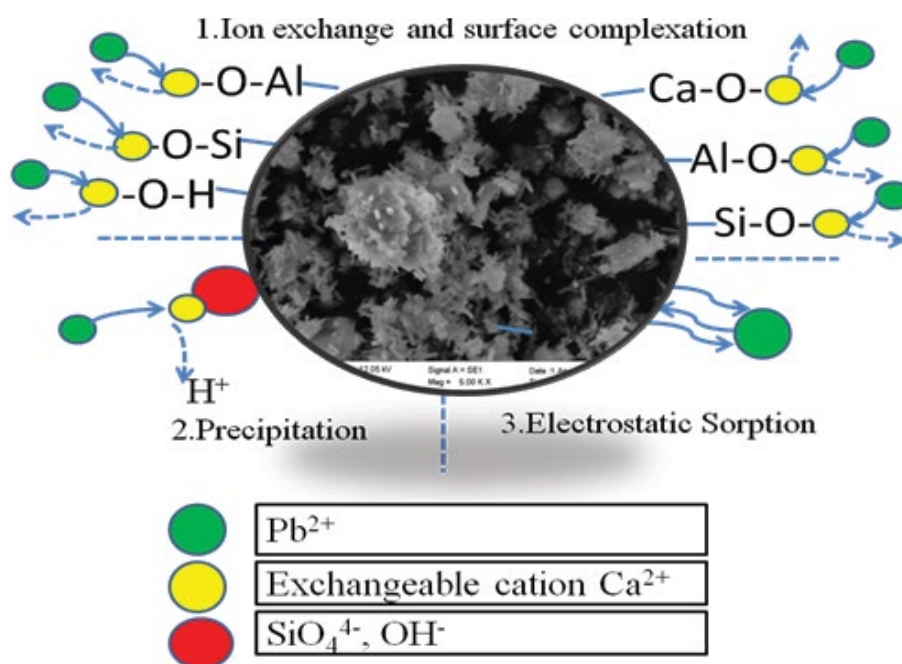Fig. 14. (a) SEM and (b) EDX after adsorbing Pb^{2+} onto Al-CSH.

Fig. 15. The schematic illustration of Pb^{2+} ions sorption mechanisms on Al-CSH.

Table 6
Removal efficiency of heay metal ions in practical industrial wastewater after contact with Al-CSH

Corp.	Heay metal ions	Concentration before adsorption (mg/g)	Concentration after adsorption (mg/g)	Removal efficiency (%)	MPC of heavy metal ions (mg/L)
1	Pb^{2+}	16.20	0.316	98.05	1.0
	Cd^{2+}	1.48	0.034	97.70	0.1
2	Pb^{2+}	35.28	0.734	97.92	1.0
	Cd^{2+}	3.63	0.086	97.63	0.1

MPC, the maximum permissible concentrations (in China).

from the eggshell, which are free. Other reagents such as industrial silica, potassium hydroxide, anhydrous acetic acid, sodium meta aluminate, and ammonium bicarbonate are purchased on the market, with the prices of 3.8, 6.5, 2.8, 3.0, and 0.65 yuan/Kg, respectively. After a rough calculation, the reagent cost in the synthesis of Al-CSH is 1.54 yuan/Kg, with low synthesis cost. The removal rate of 0.06 g Al-CSH for 100 mL 200 mg/L Pb(II) is 95.55%, and the equilibrium adsorption capacity is 318.48 mg/g. The removal effect for lead ions is significant, which proves that the practical application of Al-CSH has economic feasibility.

3.8. Application of Al-CSH in practical industrial wastewater

Based on the dynamic adsorption test method, the experimental wastewater was extracted from two local heavy metal-containing manufacturing enterprises in Hengyang, Hunan Province. The prepared Al-CSH was used as the adsorption column material, controlling the flow rate at 3 mL/min. Table 6 shows the test results. After the dynamic adsorption test, the concentrations of the three heavy metals in the treated wastewater can meet the maximum permissible concentrations of the GB8978-1996 the first-class pollutant (in China). Meanwhile, the concentration of each heavy metal ion is far below the range of China's permitted emission standards. Al-CSH can be well used in the treatment of actual heavy metal wastewater.

4. Conclusions

The results obtained from sorption experiments indicate that Al-CSH is an efficient sorbent for the removal of lead ions from solution. The removal efficiencies were significantly influenced by initial Pb(II) concentration, solution pH and contact time. The experiments have proved that:

- The optimum adsorption conditions were found to be the initial pH of 5.5, Al-CSH dosage of 0.06 g, initial Pb(II) ion concentration of 200 mg/L and contact time of 60 min. Results demonstrated that the equilibrium adsorption capacity was up to 318.48 mg/g at 313°K.
- The Langmuir adsorption isotherm model can be applied to our experimental results. The maximum adsorption capacities by Langmuir model were found to be 479.99 mg/g at 313°K.
- A floc fiber and needle-like surface of Al-CSH is the effective structure for the sorption, and the mechanism involves ion exchange with Ca^{2+}, electrostatic interactions, surface as well as complexation with $\equiv Si–OH$ and $\equiv Al–OH$ etc.
- The pseudo-second-order kinetic model was adopted to fit the adsorption process of Pb(II) onto Al-CSH. The thermodynamic parameters indicated that the adsorption was a spontaneous endothermic reaction, while the temperature increase was beneficial to the removal of Pb(II) onto Al-CSH.

Acknowledgments

References

[1] L. Bai, H. Hua, W. Fu, J. Wan, X. Cheng, L. Zhuge, L. Xiong, Q. Chen, Synthesis of a novel silica-supported dithiocarbamate adsorbent and its properties for the removal of heavy metal ions, J. Hazard. Mater., 195 (2011) 261–275.

[2] W. Fu, X. Wang, Z. Huang, Remarkable reusability of magnetic Fe_3O_4-encapsulated $C_3N_3S_3$ polymer/reduced graphene oxide composite: a highly effective adsorbent for Pb and Hg ions, Sci. Total Environ., 659 (2019) 895–904.

[3] W. Fu, H. Chen, S. Yang, W. Huang, Z. Huang, Poly(diallyldimethylammonium-MoS_4) based amorphous molybdenum sulphide composite for selectively mercury uptake from wastewater across a large pH region, Chemosphere, 232 (2019) 9–17.

[4] P. Bhunia, S. Chatterjee, P. Rudra, S. De, Chelating polyacrylonitrile beads for removal of lead and cadmium from wastewater, Sep. Purif. Technol., 193 (2018) 202–213.

[5] Q. Dong, X. Guo, X. Huang, L. Liu, J. Chen, Selective removal of lead ions through capacitive deionization: role of ion-exchange membrane, Chem. Eng. J., 361 (2019) 1535–1542.

[6] K. Zhang, Y. Xue, H. Xu, Y. Yao, Lead removal by phosphate solubilizing bacteria isolated from soil through biomineralization, Chemosphere, 224 (2019) 272–279.

[7] H. Khoshsang, A. Ghaffarinejad, Rapid removal of lead (II) ions from aqueous solutions by saffron flower waste as a green biosorbent, J. Environ. Chem. Eng., 6 (2018) 6021–6027.

[8] Y. Li, M.A. Abedalwafa, C. Ni, N. Sanbhal, L. Wang, Removal and direct visual monitoring of Lead(II) using amino acids functionalized polyacrylonitrile nanofibrous membranes, React. Funct. Polym., 138 (2019) 18–28.

[9] F.Y. AlJaberi, Studies of autocatalytic electrocoagulation reactor for lead removal from simulated wastewater, J. Environ. Chem. Eng., 6 (2018) 6069–6078.

[10] W. Fu, Z. Huang, Magnetic dithiocarbamate functionalized reduced graphene oxide for the removal of Cu(II), Cd(II), Pb(II), and Hg(II) ions from aqueous solution: synthesis, adsorption, and regeneration, Chemosphere, 209 (2018) 449–456.

[11] R. Krishnamoorthy, B. Govindan, F. Banat, V. Sagadevan, M. Purushothaman, P.L. Show, Date pits activated carbon for divalent lead ions removal, J. Biosci. Bioeng., 128 (2019) 88–97.

[12] Md.R. Awual, Md.Mr. Hasan, A. Islam, M.M. Rahman, A.M. Asiri, Md.A. Khaleque, Md.C. Sheikh, Offering an innovative composited material for effective lead(II) monitoring and removal from polluted water, J. Cleaner Prod., 231 (2019) 214–223.

[13] H. Yang, J. Fan, H. Tian, X. Wang, W. Fu, E. Alam, Synthesis of imprinted amino- functionalized mesoporous silica and their selective adsorption performance of Pb^{2+}, Cu^{2+}, and Zn^{2+}, J. Sol-Gel Sci. Technol., 90 (2019) 465–477.

[14] H. Yang, J. Fan, X. Wang, W. Fu, H. Tian, E. Alam, Investigation on synthesis of ion-imprinted mesoporous adsorbents by using ultrasound- and microwave-assisted preparation and their dynamic adsorption properties on heavy metals, Environ. Sci. Pollut. Res., 26 (2019) 10987–10999.

[15] W. Fu, Z. Huang, One-pot synthesis of two-dimensional porous Fe_3O_4/poly ($C_3N_3S_3$) network nanocomposite for selective removal of Pb(II) and Hg(II) from synthetic wastewater, ACS Sustainable Chem. Eng., 6 (2018) 14785–14794.

[16] H. Stade, D. Mueller, On the coordination of Al in ill-crystallized C-S-H phases formed by hydration of tricalcium silicate and by precipitation reactions at ambient temperature, Cem. Concr. Res., 17 (1987) 553–561.

[17] S. Kwan, J. La Rosa-Thompson, M.W. Grutzeck, Structures and phase relations of aluminum-substituted calcium silicate hydrate, J. Am. Ceram. Soc., 79 (1996) 967–971.

[18] R. Gabrovsek, B. Kurbus, D. Mueller, W. Weiker, Tobermorite formation in the system CaO, C_3S-SiO-Al_2O_3-NaOH-H_2O under hydrothermal conditions, Cem. Concr. Res., 23 (1993) 321–328.

[19] P. Mandaliev, E. Wieland, R. Dähn, J. Tits, S.V. Churakov, O. Zaharkoc. Mechanisms of Nd(III) uptake by 11Å tobermorite and xonotlite, Appl. Geochem., 25 (2010) 763–777.

[20] P. Mandaliev, T. Stumpf, J. Tits, R. Dähn, C. Walther, E. Wieland, Uptake of Eu(III) by 11Å tobermorite and xonotlite: A TRLFS and EXAFS study, Geochim. Cosmochim. Acta, 75 (2011) 2017–2029.

[21] H. Katsumata, S. Kaneco, R. Matsuno, K. Itoh, K. Masuyama, T. Suzuki, K. Funasaka, K. Ohta, Removal of organic polyelectrolytes and their metal complexes by adsorption onto xonotlite, Chemosphere, 52 (2003) 909–915.

[22] N.Y. Mostafa, E.A. Kishar, S.A. Abo-El-Enein, FTIR study and *cation exchange* capacity of Fe³⁺- and Mg²⁺-substituted *calcium silicate* hydrates, J. Alloys Compd., 473 (2009) 538–542.

[23] M. Miyake, M. Iwaya, T. Suzuki, Aluminium-substituted gyrolite as cation exchanger, J. Am. Ceram. Soc., 73 (1990) 3524–3527.

[24] M. Tsuji, S. Komarneni, P. Malla, Substituted tobermorites: 27Al and 29Si MASNMR, cation exchange, and water sorption studies, J. Am. Ceram. Soc., 74 (1991) 274–276.

[25] F. Liu, X. Wang, J. Cao, Effect of ultrasonic process on carbide slag activity and synthesized xonotlite, Phys. Procedia, 25 (2012) 56–62.

[26] J. Zou, C. Guo, Y. Jiang, C. Wei, F. Li, Structure, morphology and mechanism research on synthesizing xonotlite fiber from acid-extracting residues of coal fly ash and carbide slag, Mater. Chem. Phys., 172 (2016) 121–128.

[27] K. Lin, J. Chang, G. Chen, M. Ruan, C. Ning, A simple method to synthesize single-crystalline β-wollastonite nanowires, J. Cryst. Growth, 300 (2007) 267–271.

[28] Z. Zhang, X. Wang, H. Wang, J, Zhao, Removal of Pb(II) from aqueous solution using hydroxyapatite/calcium silicate hydrate (HAP/C-S-H) composite adsorbent prepared by a phosphate recovery process, Chem. Eng. J., 344 (2018) 53–61.

[29] R. Bardestani, C. Roy, S. Kaliaguine, The effect of biochar mild air oxidation on the optimization of lead(II) adsorption from wastewater, J. Environ. Manage., 240 (2019) 404–420.

[30] P.S. Chen, C. Qin, T. Wang, F. Chen, X. Li, H. Hou, M. Zhou, Study on the adsorption of dyestuffs with different properties by sludge-rice husk biochar: adsorption capacity, isotherm, kinetic, thermodynamics and mechanism, J. Mol. Liq., 285 (2019) 62–74.

[31] M.d.M. Orta, J. Martín, S. Medina-Carrasco, J.L. Santos, I. Aparicio, E. Alonso, Adsorption of propranolol onto montmorillonite: kinetic, isotherm and pH studies, Appl. Clay Sci., 173 (2019) 107–114.

[32] G.S. Maia, J.R. de Andrade, M.G.C. da Silva, M.G.A. Vieira, Adsorption of diclofenac sodium onto commercial organoclay: kinetic, equilibrium and thermodynamic study, Powder Technol., 345 (2019) 140–150.

[33] V.G.D. Değermenci, N. Değermenci, V. Ayvaoğlu, E. Durmaz, D. Çakır, E. Akan, Adsorption of reactive dyes on lignocellulosic waste; characterization, equilibrium, kinetic and thermodynamic studies, J. Cleaner Prod., 225 (2019) 1220–1229.

[34] J. Zhao, Y. Zhu, J. Wu, J. Zheng, X. Zhao, B. Lu, F. Chen, Chitosan-coated mesoporous microspheres of calcium silicate hydrate: environmentally friendly synthesis and application as a highly efficient adsorbent for heavy metal ions, J. Colloid Interface Sci., 418 (2014) 208–215.

[35] G. Qi, H. Ren, H. Fan, Y. Liu, Preparation of CoFe₂O₄ nanoparticles based on high-gravity technology and application for the removal of lead, Chem. Eng. Res. Des., 147 (2019) 520–528.

[36] M.-E. Lee, J.H. Park, J.W. Chung, Comparison of the lead and copper adsorption capacities of plant source materials and their biochars, J. Environ. Manage., 236 (2019) 118–124.

[37] A.M. Georgescu, F. Nardou, V. Zichil, I.D. Nistor, Adsorption of lead(II) ions from aqueous solutions onto Cr-pillared clays, Appl. Clay Sci., 152 (2018) 44–50.

[38] V.B. Cashin, D.S. Eldridge, P. Kingshott, A. Yu, Distinguishing surface sites involved in the adsorption of lead onto sinapinaldehyde-functionalised mesocellular foam mesoporous silica, Colloids Surf., A, 552 (2018) 153–160.

[39] F.K. Mahar, L. He, K. Wei, M. Mehdi, M. Zhu, J. Gu, K. Zhang, Z. Khatri, I. Kim, Rapid adsorption of lead ions using porous carbon nanofibers, Chemosphere, 225 (2019) 360–367.

[40] P. Pal, A. Pal, Treatment of real wastewater: kinetic and thermodynamic aspects of cadmium adsorption onto surfactant-modified chitosan beads, Int. J. Biol. Macromol., 131 (2019) 1092–1100.

[41] S.A. Koksharov, S.V. Aleeva, O.V. Lepilova, Description of adsorption interactions of lead ions with functional groups of pectin-containing substances, J. Mol. Liq., 283 (2019) 606–616.

[42] R. Soltani, A. Marjani, S. Shirazian, Facile one-pot synthesis of thiol-functionalized mesoporous silica submicrospheres for Tl(I) adsorption: Isotherm, kinetic and thermodynamic studies, J. Hazard. Mater., 371 (2019) 146–155.

[43] W. Guan, F. Ji, D. Fang, Y. Cheng, Z. Fang, Q. Chen, P. Yan, Porosity formation and enhanced solubility of calcium silicate hydrate in hydrothermal synthesis, Ceram. Int., 40 (2014) 1667–1674.

[44] S. Ding, D. Fang, Z. Pang, B. Luo, L. Kuang, H. Wang, Q. Zhang, Q. Shen, F. Ji, Immobilization of powdery calcium silicate hydrate via PVA covalent cross-linking process for phosphorus removal, Sci. Total Environ., 645 (2018) 937–945.

[45] D. Hou, Z. Lu, T. Zhao, Q. Ding, Reactive molecular simulation on the ordered crystal and disordered glass of the calcium silicate hydrate gel, Ceram. Int., 42 (2016) 4333–4346.

[46] D. Lee, Formation of leadhillite and calcium lead silicate hydrate (C-Pb-S-H) in the solidification/stabilization of lead contaminants, Chemosphere, 66 (2007)1727–1733.

[47] R. Zak, J. Deja, Spectroscopy study of Zn, Cd, Pb and Cr ions immobilization on C-S-H phase, Spectrochim. Acta, Part A, 134 (2015) 614–620.

[48] D. Zhao, Y. Gao, S. Nie, Z. Liu, F. Wang, P. Liu, S. Hu, Self-assembly of honeycomb-like calcium-aluminum-silicate-hydrate (C-A-S-H) on ceramsite sand and its application in photocatalysis, Chem. Eng. J., 344 (2018) 583–593.